scientific reports

OPEN

Investigation of the crystallization process of CSD-ErBCO on IBAD-substrate via DSD approach

R. Hayasaka[1]✉, P. Cayado[2]✉, M. Erbe[2]✉, W. Freitag[2], J. Hänisch[2], B. Holzapfel[2], S. Ito[1] & H. Hashizume[1]

REBa$_2$Cu$_3$O$_{7-\delta}$ (REBCO, RE: rare earth, such as Y and Gd) compounds have been extensively studied as a superconducting layer in coated conductors. Although ErBCO potentially has better superconducting properties than YBCO and GdBCO, little research has been made on it, especially in chemical solution deposition (CSD). In this work, ErBCO films were deposited on IBAD (ion-beam-assisted-deposition) substrates by CSD with low-fluorine solutions. The crystallization process was optimized to achieve the highest self-field critical current density (J_c) at 77 K. Commonly, for the investigation of a CSD process involving numerous process factors, one factor is changed keeping the others constant, requiring much time and cost. For more efficient investigation, this study adopted a novel design-of-experiment technique, definitive screening design (DSD), for the first time in CSD process. Two different types of solutions containing Er-propionate or Er-acetate were used to make two types of samples, Er-P and Er-A, respectively. Within the investigated range, we found that crystallization temperature, dew point, and oxygen partial pressure play a key role in Er-P, while the former two factors are significant for Er-A. DSD revealed these significant factors among six process factors with only 14 trials. Moreover, the DSD approach allowed us to create models that predict J_c accurately. These models revealed the optimum conditions giving the highest J_c values of 3.6 MA/cm^2 for Er-P and 3.0 MA/cm^2 for Er-A. These results indicate that DSD is an attractive approach to optimize CSD process.

ErBa$_2$Cu$_3$O$_{7-\delta}$ (ErBCO) is one of the REBa$_2$Cu$_3$O$_{7-\delta}$ (REBCO, RE: rare earth) compounds with potential as a functional superconducting layer in coated conductors[1,2]. Indeed, Yoshida et al. have demonstrated ErBCO coated conductor samples of nearly 100 m length with average critical current values, I_c, of ~ 700 A/cm-width[3]. Most of the film studies on ErBCO were done via PLD[4] (pulsed laser deposition) especially regarding possible enhancement of the critical current density, J_c, by perovskite nanoparticles[5] and nanorods[6]. Just occasional ErBCO film studies are reported for other vacuum (MOCVD[7], sputtering[8]) and non-vacuum methods (CSD/MOD (metal–organic deposition)[9,10], sol–gel[11]). Since the ion sizes of Er^{3+} and Y^{3+} are very similar, the stability and growth temperatures of ErBCO and YBCO are well comparable[12], differing by only ~ ± 10 °C. In this work, since few research has been made on ErBCO CSD process, we prepared ErBCO films on technical IBAD templates[13] by CSD[14,15], following the TFA-MOD (metal–organic deposition of trifluoroacetates) route with low-fluorine solutions[16,17].

In order to find the optimum process conditions for complicated systems such as CSD, one has to deal with numerous parameters, requiring a lot of time and cost for try and error. In particular, the thermal processes involved in CSD have conventionally been optimized in one-factor-at-a-time experiments, i.e., only one of the potentially important parameters is changed, keeping all the others constant. This kind of investigation is extensive and often incomplete because significant parameters, i.e., those influencing and determining the final quality of the films, are often correlated. For example, in CSD, the optimum crystallization temperatures are reported to depend on the oxygen partial pressure[18]. The one-factor-at-a-time approach often fails to find

[1]Graduate School of Engineering, Department of Quantum Science and Energy Engineering, Tohoku University, Aramaki-Aza-Aoba 6-6-01-2, Aoba-ku, Sendai, Miyagi 980-8579, Japan. [2]Karlsruhe Institute of Technology (KIT), Institute for Technical Physics (ITEP), Hermann-von-Helmholtz-Platz 1, 76344 Eggenstein-Leopoldshafen, Germany. ✉email: long.hayasaka.6832@gmail.com; pablo.cayado@kit.edu; manuela.erbe@kit.edu

Level (coded units)	T_{crys} (°C)	p_{oxy} (ppm)	T_{Dew} (°C)	Dewll time (min)	Heating ramp (°C/min)	Rotation speed (rpm)
Low (−1)	770	150	16	38	10	2000
Medium (0)	780	225	19	64	15	3000
High (1)	790	300	22	90	20	4000

Table 1. Investigated factors and their levels.
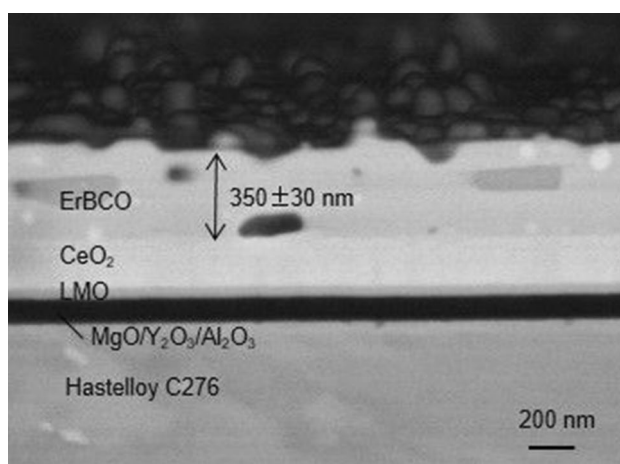
Figure 1. The cross-section of an Er-P sample deposited with 3000 rpm. Buffer layers of MgO/Y$_2$O$_3$/Al$_2$O$_3$ delaminated in the course of the cross-section preparation.

such interactions and requires many experiments to improve process conditions. Therefore, we adopted a novel design-of-experiment (DOE) technique, Definitive Screening Design (DSD)[19] for the first time, to identify significant factors and improve self-field critical current density, J_c^{sf}, at 77 K while reducing the number of necessary experiments as much as possible.

DSD was introduced by Jones and Nachtsheim in 2011[19]. It offers the opportunity to investigate many parameters and optimize a process by performing one experiment with a small number of trials[20,21]. Among the multitude of possible combinations of levels (magnitudes) of the preselected parameters (called "factors"), DSD identifies the few trials to be performed for efficient evaluation of the factors' effects. Main effects (the first-order effect of a single factor), two-factor interactions (the correlation between two factors), and quadratic effects are estimable at the same time. This feature distinguishes DSD from other, conventional DOE techniques, most of which cannot estimate quadratic effects or need many trials to estimate them. This advantage of DSD makes it possible to find the optimum condition in a large experimental space. By using DSD, one can understand how the target value is changed by the levels of the factors, identify important factors, and finally optimize their levels.

Experimental

Solution and sample preparation. The low-fluorine solutions of this study are prepared by mixing fluorinated and non-fluorinated precursor salts, namely Er-propionate or Er-acetate, Ba-TFA, and Cu-propionate, in the stoichiometric ratio Er:Ba:Cu = 1:2:3 in anhydrous methanol resulting in a concentration of 1.5 M (sum of metals). Two types of ErBCO samples were prepared from two different solutions depending on the Er precursor salt ("Er-P" samples from Er-propionate and "Er-A" samples from Er-acetate). The solutions were deposited on 10 × 10 mm^2 IBAD substrates by spin coating for 30 s at different rotation speeds (2000–4000 rpm). The SuperOx IBAD substrates had the architecture of CeO$_2$/LaMnO$_3$ (LMO)/MgO/Y$_2$O$_3$/Al$_2$O$_3$/Hastelloy C276. The details of the standard pyrolysis and crystallization steps are available in Ref.[22]. The investigated factors were crystallization temperature (T_{crys}), oxygen partial pressure (p_{oxy}), dew point (T_{Dew}), heating ramp, dwell time, and rotation speed. The investigated ranges of these factors and levels are listed in Table 1. We have chosen these parameters because they are known by experience to be the most important parameters that affect the film growth and are directly controllable with our equipment (furnace and spin coater). Other factors might be considered; however, from our experience, we can assume there are no factors that correlate with the six factors in this experiment. That is, these six factors do not have to be considered with other possible factors at the same time.

Thin-film characterization. The film thicknesses for the rotation speeds of 2000, 3000, and 4000 rpm were 400, 350, and 285 nm, respectively, as analyzed with cross-sectional scanning electron microscopy by a LEO 1530 scanning electron microscope (SEM) with field emission gun (0.1 kV and 30 kV) by *Zeiss*. Figure 1 shows an example of the cross-section of an Er-P sample deposited with 3000 rpm, and the thickness of ErBCO

	Coded units of factors					
Sample	T_{crys}	p_{oxy}	T_{Dew}	Dewll time	Heating ramp	Rotation speed
1	0	1	1	1	1	1
2	0	− 1	− 1	− 1	− 1	− 1
3	1	0	1	1	1	1
4	− 1	0	− 1	− 1	− 1	− 1
5	1	1	0	1	1	1
6	− 1	− 1	0	− 1	− 1	− 1
7	1	1	1	0	1	1
8	− 1	− 1	− 1	0	− 1	− 1
9	1	1	1	1	0	1
10	− 1	− 1	− 1	− 1	0	− 1
11	1	1	1	1	1	0
12	− 1	− 1	− 1	− 1	− 1	0
13 (center run)	0	0	0	0	0	0
14 (center run)	0	0	0	0	0	0

Table 2. The design matrix with coded units (− 1, 0, 1), which correspond to the levels in Table 1. The run in the bottom row (center run) was repeated to estimate the population variance regardless of significant factors.

is 350 ± 30 nm. The variation of the thickness is about 10% of the total thickness. Self-field J_c (J_c^{sf}) at 77 K was measured inductively with a Cryoscan (Theva, 50 µV criterion).

Definitive screening design and model selection. The design matrix for the investigated factors, Table 2, is generated by using a so-called conference matrix[23]. Coded units (− 1, 0, and 1) correspond to the levels in Table 1. The trials (runs) are carried out using the parameter sets (rows) specified in Table 2 in random order. The minimum number of runs is $2K + 1 = 13$ (K is the number of factors), but the runs with level 0 of all factors (center run) was repeated, see bottom rows of Table 2. This repetition of the center run is necessary to estimate the population variance regardless of significant factors. Without the repetition of this center run or addition of fake factors[24], the population variance has to be estimated by the residual sum of squares of the model containing significant parameters; hence, the estimator of the variance will not be unique but dependent on the chosen model.

After obtaining the experimental data, models are built following an appropriate model selection procedure. The data included in the model are the values of the property to be optimized, such as J_c at a certain magnetic field, a ratio of J_c at different fields and/or temperatures, or critical temperature T_c. Although the model and its predictions depend on the selected property, we construct the model regarding J_c^{sf} at 77 K in this work. The best second-order model (containing main, interaction, and quadratic effects) was selected among all the possible second-order models based on the Akaike information criterion with finite correction (AICc). AICc (or generally AIC) is an estimator to select a "good" model avoiding overfitting, which can explain the prediction values well. Supposing that the errors follow independent and identical normal distributions, AICc is expressed in the following equation for the least square estimation[23].

$$\text{AICc} = n \ln \left(\hat{\sigma}^2 \right) + 2K + \frac{2K(K+1)}{n - K - 1} \tag{1}$$

where n is the number of observations and $\hat{\sigma}^2$ is the estimator of the variance calculated by

$$\hat{\sigma}^2 = \frac{\Sigma \left(y_i - \widehat{y_i} \right)^2}{n} \tag{2}$$

where y_i and $\widehat{y_i}$ are observed and fitted value, respectively, of the ith factor.

Results and discussion

Table 3 shows the J_c^{sf} values at 77 K of Er-P and Er-A samples for the DSD experiment (Samples 1–14) together with pilot trials (Samples 15–30) that were obtained before starting the DSD experiment and used for confirmation of the equations (models) later. In the DSD experiment, the J_c^{sf} values at 77 K ranged from 0 to 3.67 MA/cm² for Er-P, and from 0 to 3.30 MA/cm² for Er-A. Considering the measured thickness variation of about ± 30 nm (~ 10% of ErBCO layer), the J_c values also have an uncertainty of about ± 10%.

Among all the possible second-order models containing main, interaction, and quadratic effects, the models with minimum AICc, Eqs. (3) and (4), were selected for Er-P and Er-A respectively. Samples 1–14 were used to create these models.

$$J_c(\text{Er - P}) = 2.737 - 0.417 \left(T_{crys} - 780 \right)/10 + 0.531 \left(p_{oxy} - 225 \right)/75 - 0.623 (T_{Dew} - 19)/3 - 0.654 \left\{ \left(p_{oxy} - 225 \right)/75 \right\}^2 \tag{3}$$

Sample	T_{crys} [°C]	p_{oxy} [ppm]	T_{Dew} [°C]	Dwell time [min]	Heating ramp [°C/h]	Rotation speed [rpm]	J_c^{sf} at 77 K (Er-P) [MA/cm²]	J_c^{sf} at 77 K (Er-A) [MA/cm²]
1	780	300	22	90	20	4000	1.99	1.91
2	780	150	16	38	10	2000	2.35	2.13
3	790	225	22	38	10	4000	2.17	0
4	770	225	16	90	20	2000	3.35	2.13
5	790	300	19	90	10	2000	2.42	1.08
6	770	150	19	38	20	4000	2.76	1.17
7	790	150	22	64	20	2000	0	0
8	770	300	16	64	10	4000	3.67	2.93
9	790	150	16	90	15	2000	1.81	1.98
10	770	300	22	38	15	4000	2.47	0.33
11	790	300	16	38	20	3000	2.52	1.29
12	770	150	22	90	10	3000	0.84	0.23
13	780	225	19	64	15	3000	2.6	2.19
14	780	225	19	64	15	3000	2.83	1.97
15	780	225	19	64	20	2000	2.68	2.64
16	790	225	19	64	20	2000	1.06	–
17	780	225	19	64	20	3000	1.80	–
18	770	300	16	90	20	3000	3.17	–
19	770	275	16	38	20	4000	3.37	–
20	770	300	16	90	20	2000	2.95	–
21	770	150	22	90	10	3000	0.33	–
22	770	300	22	38	15	2000	1.99	–
23	770	300	16	90	20	3000	2.82	–
24	770	300	16	90	20	3000	2.97	–
25	770	256	16	64	15	3000	3.21	–
26	770	256	16	64	15	4000	3.61	–
27	780	225	19	64	10	2000	–	2.45
28	780	225	19	64	15	3000	–	2.19
29	770	275	16	38	20	3000	–	2.21
30	778.5	225	16	64	15	3000	–	2.88
31	778.5	225	16	64	15	4000	–	3.07

Table 3. Measured J_c^{sf} at 77 K of Er-P and Er-A. The latter twelve samples (below the bold line) are for the confirmation of the models [Eqs. (3) and (4)].

Term	Coefficient	Standard error	P value
J_c (Er-P)			
Intercept	2.737	0.221	<0.001
T_{crys}	−0.417	0.140	0.015
p_{oxy}	0.531	0.140	0.004
T_{Dew}	−0.623	0.140	0.002
$(p_{oxy})^2$	−0.654	0.261	0.034
J_c (Er-A)			
Intercept	2.049	0.226	<0.001
T_{crys}	−0.303	0.143	0.060
T_{Dew}	−0.739	0.143	<0.001

Table 4. The statistical description of the model for J_c(Er-P) and J_c (Er-A). The coefficients are expressed in the coded units. The tables describe only the significant terms with P-value[24] smaller than 0.05.

$$J_c(\text{Er - A}) = 2.049 - 0.303\left(T_{crys} - 780\right)\big/10 - 0.739(T_{Dew} - 19)\big/3 - 0.876\left\{\left(T_{crys} - 780\right)\big/10\right\}^2 \quad (4)$$

Table 4(a) and (b) list the important factors of these models for J_c^{sf} at 77 K with P values of the coefficients (the smaller the P value is, the more likely the coefficient is not zero, hence, significant). The significant main factors for Er-P are T_{crys}, p_{oxy}, and T_{Dew}, while for Er-A only T_{crys} and T_{Dew}. Dwell time, heating ramp, and rotation speed
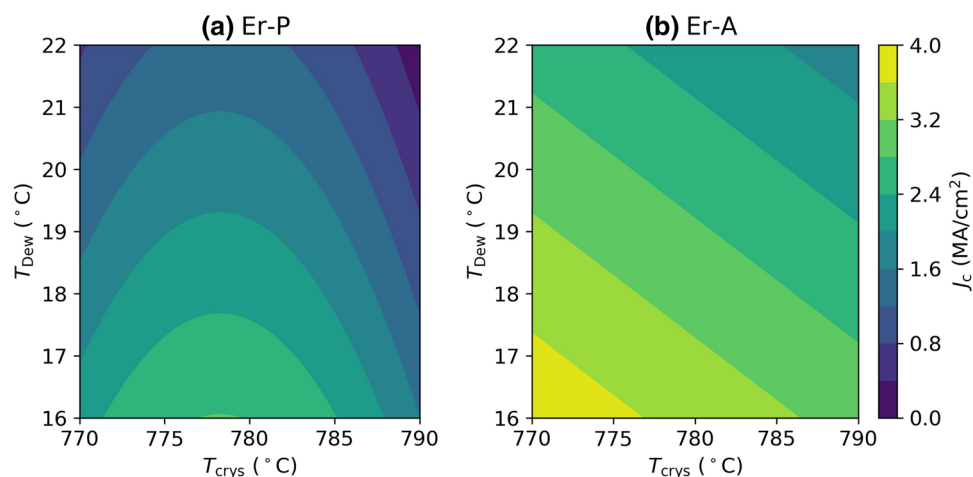
Figure 2. The behavior of (**a**) J_c (Er-P) and (**b**) J_c (Er-A) over humidity and T_{crys}. In (**b**), p_{oxy} is fixed as the optimal level of 256 ppm (0.413 in coded unit) for J_c (Er-P).
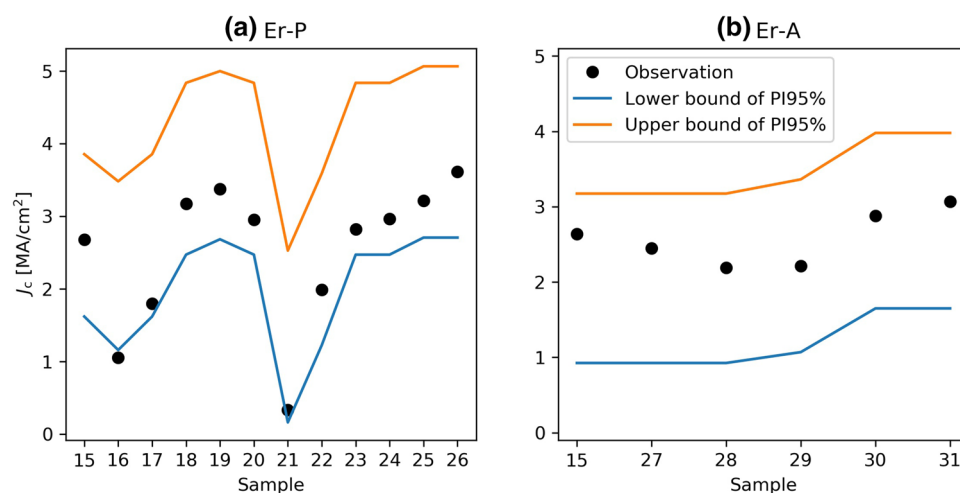
Figure 3. Model confirmation for (**a**) J_c (Er-P) and (**b**) J_c (Er-A). The conditions of the samples are described in Table 3. Samples 25 and 26 are optimal Er-P samples, Samples 30 and 31 are optimal Er-A samples. Note that measured J_c values have an uncertainty of about 10% because of the thickness uncertainty.

are not significant for both sets of samples. The quadratic effect of p_{oxy} is significant for Er-P, and the quadratic effect of T_{crys} for Er-A. Neither of the two sets of samples showed any sign of two-factor interactions. Since at least some of the factors are usually correlated (e.g., the interaction between T_{crys} and p_{oxy} is certainly present[18]), we conclude that the investigated range in this work was not wide enough to detect such interactions.

Based on these models, Eqs. (3) and (4), the dependencies of J_c (Er-P) and J_c (Er-A) on T_{Dew} and T_{crys} are visualized in Fig. 2. Figure 2a shows that lower T_{crys} and lower T_{Dew} are crucial for improving J_c (Er-P) with the optimal $p_{oxy} = 256$ ppm (0.413 in coded unit), whereas Fig. 2b shows intermediate T_{crys} and lower T_{Dew} to be crucial for J_c (Er-A). The major differences between both sample types are that the desirable T_{crys} is lower for Er-P than for Er-A, and p_{oxy} is a significant parameter (in the investigated range) for Er-P but not for Er-A.

To confirm the validity of the J_c (Er-P) model Eq. (3), further twelve Er-P samples were selected (Samples 15–26 in Table 3) and their J_c^{sf} values at 77 K measured. Figure 3a shows these J_c (Er-P) values together with their 95% prediction intervals (PI95%). Most of the data fall inside this prediction interval. Hence, the model is considered useful to predict J_c (Er-P). Furthermore, the model suggests that the maximum range of J_c^{sf} at 77 K (2.9–4 MA/cm^2) can be obtained with $T_{crys} = 770$ °C, $p_{oxy} = 256$ ppm, $T_{Dew} = 16$ °C (other parameters are arbitrary values). The samples made with these conditions are Sample 25 (3.2 MA/cm^2) and Sample 26 (3.6 MA/cm^2), which are indeed the highest level (considering 10% uncertainty of J_c) and inside the prediction interval in Fig. 3a Similarly, the validation of J_c (Er-A) has been checked using Sample 15, and Samples 27–31 in Fig. 3b The optimal samples are Samples 30 and 31 prepared with $T_{crys} = 778.5$ °C and $T_{Dew} = 16$ °C (other parameters are not important). Samples 30 and 31 certainly outperformed the other Er-A samples.

Moreover, since not all the factors have quadratic effects, the global optimum seems to exist outside of the investigated range in this work. However, a one-factor-at-a-time approach for further improvement is acceptable because the interactions between the significant factors (T_{crys}, p_{oxy}, and T_{Dew}) are not likely to be present near the investigated range.

Conclusion

The crystallization process of ErBCO films deposited with CSD on SuperOx IBAD substrates was optimized via DSD, a novel design-of-experiment technique. This approach allowed investigating the effects of six crystallization parameters (T_{crys}, p_{oxy}, T_{Dew}, dwell time, heating ramp, and rotation speed) with a considerably reduced number of trials compared to conventional one-factor-at-a-time approach. The crystallization was optimized regarding J_c^{sf} at 77 K. Two types of ErBCO samples, Er-P and Er-A, prepared from the solutions containing Er-propionate and Er-acetate, respectively, were studied. Only 14 samples per sample type were necessary for this DSD experiment. The models based on the experiment reveal that T_{crys}, p_{oxy}, and T_{Dew} are significant factors for J_c (Er-P), and only T_{crys} and T_{Dew} for J_c (Er-A) in the investigated range of the factors. As expected from the model for J_c (Er-P), a maximum of ~ 3.6 MA/cm^2 was obtained with $T_{crys} = 770$ °C, $p_{oxy} = 256$ ppm, and $T_{Dew} = 16$ °C. Similarly, a maximum J_c (Er-A) of ~ 3.0 MA/cm^2 was obtained with $T_{crys} = 778.5$ °C and $T_{Dew} = 16$ °C. Both models were confirmed by additional samples. These results indicate that DSD is a very attractive approach to optimize the properties of CSD-grown films. It could also be a powerful tool for the development of long-tape coated conductors as it could enormously reduce the effort in the optimization of the different process steps.

References

1. Obradors, X. *et al.* Coated conductors for power applications: materials challenges. *Supercond. Sci. Technol.* **27**, 044003 (2014).
2. Bondarenko, S. I., Koverya, V. P., Krevsun, A. V. & Link, S. I. High-temperature superconductors of the family (RE) Ba$_2$Cu$_3$O$_{7-\delta}$ and their application. *Low Temp. Phys.* **43**, 1125–1151 (2017).
3. Yoshida, T. *et al.* Fabrication of 93.7 m long PLD-EuBCO+ BaHfO$_3$ coated conductors with 103 A/cm W at 77 K under 3 T. *Phys. C Supercond. Appl.* **518**, 54–57 (2015).
4. Ohazama, T. *et al.* Growth of high-quality ErBa$_2$Cu$_3$O$_{7-\delta}$ thin films. *Physica C Supercond. Appl.* **412–414**, 1301–1305 (2004).
5. Ito, M. *et al.* Microstructure of ErBa$_2$Cu$_3$O$_{7-\delta}$ films with BaZrO3 dispersion pinning centers for high JC applications. *Phys. C Supercond. Appl.* **426–431**, 1415–1418 (2005).
6. Kai, H. *et al.* Superconducting properties and microstructure of PLD-ErBa$_2$Cu$_3$O$_{7-\delta}$ film with BaNb$_2$O$_6$. *Phys. C Supercond. Appl.* **463–465**, 895–899 (2007).
7. Takemoto, J. H. *et al.* Microstrip resonators using two-sided metalorganic chemical vapor deposited Er–Ba–Cu–O thin films. *Appl. Phys. Lett.* **58**, 1109–1111 (1991).
8. Mochiku, T., Kanke, Y., Wen, Z., Iguchi, I. & Yamaka, E. Effect of substrate temperature on the crystalline state of Ba$_2$ErCu$_3$O$_{7-x}$ superconducting thin films by RF magnetron sputtering. *Jpn. J. Appl. Phys.* **27**, L1679–L1682 (1988).
9. Iguchi, T. *et al.* Metal–organic deposition of RE–Ba–Cu–O (RE=Dy, Ho, Er, and Tm) films using trifluoroacetates. *Physica C Supercond. Appl.* **392–396**, 900–904 (2003).
10. Manuela, E. & Cayado, P. Comparative study of CSD-grown REBCO films with different rare earth elements—part one: processing windows and Tc. *Supercond. Sci. Technol.* **11**, 1–12 (2020).
11. El-Kawni, M. I., Mutlu, I. H., Aslanoglu, Z., Akin, Y. & Hascicek, Y. S. Nonvacuum Er-123 films on buffer layered Ni tapes: processing, growth, and properties. *J. Supercond. Nov. Magn.* **15**, 191–194 (2002).
12. Salinas-Sanchez, A., Garcia-Muñoz, J. L., Rodriguez-Carvajal, J., Saez-Puche, R. & Martinez, J. L. Structural characterization of R$_2$BaCuO$_5$ (R = Y, Lu, Yb, Tm, Er, Ho, Dy, Gd, Eu and Sm) oxides by X-ray and neutron diffraction. *J. Solid State Chem.* **100**, 201–211 (1992).
13. Lee, S. *et al.* Development and production of second generation high T c superconducting tapes at SuperO$_x$ and first tests of model cables. *Supercond. Sci. Technol. Supercond. Sci. Technol* **27**, 9 (2014).
14. Obradors, X. *et al.* Progress towards all-chemical superconducting YBa$_2$Cu$_3$O$_7$-coated conductors. *Supercond. Sci. Technol.* **19**, S13–S26 (2006).
15. Izumi, T. *et al.* Progress in development of advanced TFA-MOD process for coated conductors. *Phys. C Supercond. Appl.* **463**, 510–514 (2007).
16. Li, M. *et al.* Rapid pyrolysis of SmBa$_2$Cu$_3$O$_{7-\delta}$ films in CSD-MOD using extremely-low-fluorine solutions. *Coatings* **10**, 31 (2020).
17. Palmer, X. *et al.* Solution design for low-fluorine trifluoroacetate route to YBa$_2$Cu$_3$O$_7$ films. *Supercond. Sci. Technol.* **29**, 024002 (2016).
18. Cayado, P. *et al.* Chemical solution deposition of Y1-:XGdxBa$_2$Cu$_3$O$_{7-\delta}$–BaHfO$_3$ nanocomposite films: combined influence of nanoparticles and rare-earth mixing on growth conditions and transport properties. *RSC Adv.* **8**, 42398–42404 (2018).
19. Jones, B. & Nachtsheim, C. J. A class of three-level designs for definitive screening in the presence of second-order effects. *J. Qual. Technol.* **43**, 1–15 (2011).
20. Libbrecht, W. *et al.* Optimization of soft templated mesoporous carbon synthesis using definitive screening design. *Chem. Eng. J.* **259**, 126–134 (2015).
21. Tai, M., Ly, A., Leung, I. & Nayar, G. Efficient high-throughput biological process characterization: definitive screening design with the Ambr250 bioreactor system. *Biotechnol. Prog.* **31**, 1388–1395 (2015).
22. Erbe, M. *et al.* Improved REBa2Cu3O7−x (RE = Y, Gd) structure and superconducting properties by addition of acetylacetone in TFA-MOD precursor solutions. *J. Mater. Chem. A* **2**, 4932 (2014).
23. Burnham, K. P. & Anderson, D. R. Multimodel inference. *Sociol. Methods Res.* **33**, 261–304 (2004).
24. Montgomery, D. C. *Design and Analysis of Experiments* (Wiley, Hoboken, 2019).

Author contributions

R.H., P.C. and J.H. wrote the main manuscript text and M.E. and W.F. contributed to conducting the experiments and analyzing the results. All authors reviewed the manuscript.

Funding

Competing interests

The authors declare no competing interests.

Additional information

Correspondence and requests for materials should be addressed to R.H., P.C. or M.E.

Reprints and permissions information is available at www.nature.com/reprints.

Publisher's note Springer Nature remains neutral with regard to jurisdictional claims in published maps and institutional affiliations.